Band Alignments, Valence Bands and Core Levels in the Tin Sulfides SnS, SnS_2 and Sn_2S_3: Experiment and Theory

Thomas J. Whittles[†], Lee A. Burton[‡], Jonathan M. Skelton[§], Aron Walsh[§], Tim D. Veal[†], Vin R. Dhanak*[,†]

[†]Stephenson Institute for Renewable Energy, University of Liverpool, Liverpool L69 7ZF, UK

[‡]Structure and Materials Laboratory, Tokyo Institute of Technology, 4259 R3-7 Nagatsuta, Midori-ku, Yokohama 226-8503, Japan

[§]Centre for Sustainable Chemical Technologies, Department of Chemistry, University of Bath, Bath BA2 7AY, UK

KEYWORDS: tin sulfides, lone pair electrons, photoemission measurements, DFT calculations, band alignments

ABSTRACT: Tin sulfide solar cells show relatively poor efficiencies despite attractive photovoltaic properties, and there is difficulty in identifying separate phases, which are also known to form during Cu_2ZnSnS_4 depositions. We present X-ray photoemission spectroscopy (XPS) and inverse photoemission spectroscopy measurements of single crystal SnS, SnS_2 and Sn_2S_3, with electronic-structure calculations from density functional theory (DFT). Differences in the XPS spectra of the three phases, including a large 0.9 eV shift between the $3d_{5/2}$ peak for SnS and SnS_2, make this technique useful when identifying phase-pure, or mixed-phase systems. Comparison of the valence band spectra from XPS and DFT reveals extra states at the top of the valence bands of SnS and Sn_2S_3, arising from the hybridization of lone pair electrons in Sn(II), which are not present for Sn(IV), as found in SnS_2. This results in relatively low ionization potentials for SnS (4.71 eV) and Sn_2S_3 (4.66 eV), giving a more comprehensive explanation as to the origin of the poor efficiencies. We also demonstrate, by means of a band alignment, the large band offsets of SnS and Sn_2S_3 from other photovoltaic materials, and highlight the detrimental effect on cell performance of secondary tin sulfide phase formation in SnS and CZTS films.

INTRODUCTION

Next-generation materials for use in thin film photovoltaics (PV) are receiving intensive study, driven by the toxicity and scarcity of components in the current leading commercial materials, cadmium telluride (CdTe) and copper indium gallium diselenide (CIGS).[1] Viable new materials should consist of readily available and environmentally friendly elements, whilst simultaneously retaining attractive PV properties. Copper zinc tin sulfide/selenide (CZTS) is one of the most auspicious contenders in this field, currently holding a record conversion efficiency of 12.6%.[2] As well as CZTS, several binary compounds also fulfill these criteria in their own right. Of interest here is tin sulfide (SnS), which is also important with regard to CZTS development because it is commonly used as a precursor for CZTS growth,[3–5] and is sometimes observed to form as an unwanted secondary phase.[6–10]

SnS was first realized as a promising PV absorber in 1997,[11] and has a bandgap of 1.1-1.5 eV,[12,13] a high optical absorption coefficient,[14,15] and intrinsic *p*-type conductivity.[16] Thin-film deposition methodologies for preparing SnS are many and varied, with sulfurization,[17] sputtering,[18] electrochemical deposition,[19] spray pyrolysis,[20] and thermal evaporation,[21] having been successful, amongst others. Despite this, fabricated devices have almost exclusively shown conversion efficiencies below 4%,[20–23] with the record being only 4.36%.[24] It has been suggested that poor band alignment in commonly-used device structures is the reason for these low efficiencies,[22] with a previous study, in which the band positions of SnS were determined by density functional theory (DFT), supporting this.[25] Also, three phases of tin sulfide are known to form (SnS, SnS_2, Sn_2S_3),[26] and as phase impurities, these could also be detrimental to cell performance, as discussed in our previous, theoretical study.[27] On the other hand, SnS_2 has potential as a water-splitting photocatalyst,[28] with a photon-to-current conversion efficiency of 38.7%,[29] and Sn_2S_3 could have as yet unknown applications as it is relatively poorly studied.[30]

Tin is able to form two oxidation states, Sn(II) ($[Kr]4d^{10}5s^25p^0$) and Sn(IV) ($[Kr]4d^{10}5s^05p^0$), with SnS and SnS_2 containing Sn in each of these single oxidation states respectively, whilst in Sn_2S_3, Sn adopts a mixed oxidation state, i.e. Sn(II)Sn(IV)S_3.[31] Such differences in the electronic structures lead to contrasting material properties

between the phases. Indeed, both SnS_2 and Sn_2S_3 display *n*-type conductivity,[32,33] arising from the dominant sulfur vacancy associated with the Sn(IV) oxidation state.[27] Conversely, the *p*-type conductivity of SnS[34] is attributed to the dominant tin vacancy associated with the Sn(II) oxidation state.[27] Thus, confidence in the identification of the three phases is paramount, including where these occur as impurities. Utilizing spectroscopic or diffraction techniques is, however challenging due to difficulties in the assignment of different phases and in identifying mixed-phase systems.[35–41] It is therefore necessary to study the separate phases in isolation, so that methods for robust identification and discrimination can be developed, and the possible effects of the presence of phase impurities can be investigated.

In the SnS_2 crystal structure, Sn(IV) coordinates to 6 S ions in regular octahedra. However in SnS, Sn(II) coordinates to three S ions, with a stereochemically-active lone pair of electrons occupying the final tetrahedral site.[26] This lone pair does not contribute to the bonding, but causes a distortion of the lattice.[30] Sn_2S_3 is a 1:1 combination of these crystal structures.[42] It is expected that insights into the relatively poor efficiencies of SnS PV cells can be provided by studying the effects that this uncommon bonding environment has upon the electronic structure of the material.

In this report, we present the identification of the three distinct tin sulfide phases by performing photoemission spectroscopy (PES) measurements on single crystals. We also compare the measured and theoretical valence band spectra and perform a band alignment between the three phases, relating the differences between them to the underlying electronic structure. Finally, we also discuss the possible effects of tin sulfide phase impurities in both SnS and CZTS films on PV device performance in terms of the electronic structure and band alignment.

METHODS

Experimental

Single crystals of SnS, SnS_2 and Sn_2S_3 were synthesized by iodine-assisted chemical vapor transport, and were shown to be phase-pure and of the correct stoichiometry.[27] Individual phases were visually identified by the nature of the crystals, with SnS being dark grey, SnS_2 forming yellow flakes, and Sn_2S_3 crystallizing as shiny black needles. These observations are in agreement with other studies.[38]

PES measurements were performed in a standard ultra-high vacuum (UHV) chamber operating at a base pressure of less than 2×10^{-10} mbar with hydrogen as the main residual gas. Crystals were selected for measurement using ceramic tweezers and affixed to the sample plate by pressing them firmly onto double-sided carbon tape. They were then cleaved using a steel blade in order to obtain a fresh surface. In vacuo crystal preparation was performed using an Ar^+ ion source and a radiative heating stage.

The core-level electronic structure and occupied density of states in the valence band were probed by X-ray photoemission spectroscopy (XPS) using a SPECS monochromatic Al Kα X-ray source (hν = 1486.6 eV) typically operating at 200 W, together with a PSP Vacuum Technology electron-energy analyzer operating with a typical constant pass energy of 10 eV. For measurement of the secondary electron cutoff (SEC) at low kinetic energies, the X-ray power was reduced to 9 W, the exit slit of the analyzer was reduced in size, and an arbitrarily chosen -10 V bias was applied to the sample to separate the spectrometer response. The unoccupied density of states in the conduction band was measured by inverse photoemission spectroscopy (IPES) using a PSP Vacuum Technology BaO cathode dispenser electron source and an isochromat NaCl photon detector, each mounted at an incidence angle of 45° to the sample normal.

Calibration of the spectrometers was performed using a polycrystalline silver foil, cleaned in vacuo. The Ag $3d_{5/2}$ photoelectron line had a binding energy (BE) of 368.3 eV and a full-width at half maximum (FWHM) of 0.6 eV. The Fermi edge of the silver sample had a spectral width of 0.3 eV from XPS and 0.9 eV from IPES. From these calibrations, tolerances were determined to be ±0.1 eV for core-level binding energies, ±0.05 eV for the valence band maxima (VBM) and SEC, and ±0.14 eV for the CBM. Although the cleaned samples were deemed to be free from contaminants according to the nominal sensitivity of the technique, charging of the semiconducting samples was checked by measuring the C 1s photoelectron region for many hours in order to obtain a significant signal from contaminant carbon. The C 1s photoelectron peak was found to have a BE of 285.0 eV, which was consistent across all samples and in agreement with other measurements of these materials.[43] It was thus concluded that no charging effects were observed in the spectra.

Computational Modeling

Electronic-structure calculations were carried out on the three tin sulfides within the Kohn-Sham DFT[44,45] formalism, as implemented in the Vienna ab initio simulation package (VASP) code.[46]

The room-temperature structures of each of the three tin sulfides were relaxed using the Perdew-Burke-Enzerhof (PBE) generalized-gradient approximation (GGA) functional[47] with the D3 dispersion correction applied to account for van der Waals forces;[48] the variant of the Becke-Johnson damping method was used.[49] A plane-wave basis set with a 550 eV kinetic energy cutoff was employed with projector augmented-wave (PAW) pseudopotentials[50,51] treating the Sn 5s, 4d and 5p and S 3s and 3p states as valence electrons. The Brillouin zones of SnS, SnS_2 and Sn_2S_3 were sampled using Gamma-centered Monkhorst-Pack *k*-point grids,[52] with 8×4×8, 8×8×6 and 4×8×3 subdivisions respectively. The ion positions, cell shape and volume were optimized to a tolerance of 10^{-7} eV on the electronic wavefunctions and 5×10^{-3} eV Å^{-1} on the forces.

Electronic-structure calculations were then carried out on these optimized structures using the HSE06 hybrid functional.[53–55] The electronic density of states of the valence and conduction bands was simulated using denser Brillouin zone sampling meshes with 12×6×12, 12×12×8, and

6×12×5 subdivisions (196, 131, and 84 irreducible *k*-points) for SnS, SnS_2 and Sn_2S_3, respectively, with interpolation being performed using the Blöchl-corrected tetrahedron method.[56] For these calculations, the electronic minimization was performed to a tolerance of 10^{-6} eV.

RESULTS AND DISCUSSION

Crystal Preparation

The crystals were first subjected to a cleaning procedure in an UHV chamber. 5-10 minutes of sputtering using 500 eV Ar^+ was followed by thermal annealing at 230 °C for 200, 300 and 500 minutes for SnS, SnS_2 and Sn_2S_3, respectively, in order to remove surface contamination. During cleaning, the crystals were monitored by XPS for the presence and subsequent reduction of carbon and oxygen, and were deemed to be clean when the contaminant levels fell below sensitivity and the Sn 3d spectrum demonstrated the expected peak features of the pure crystals.

During the cleaning procedures, several notable changes to the crystals were observed. SnS was found to be contaminated with iodine, remnant due to its use as the transport medium in the chemical vapor transport (CVT) synthesis;[27] this contamination was significantly reduced by the surface cleaning procedure, and therefore it was concluded that this contamination was simply surface physisorbed iodine. Neither of the other two materials showed contamination with iodine in this study, although, trace iodine was observed in Sn_2S_3 in a similar study.[38] More aggressive ion bombardment of SnS caused the formation of metallic tin on the surface, which we ascribed to the preferential sputtering of sulfur, as has been seen in similar materials.[57–61] Annealing the SnS_2 crystals at higher temperatures and for longer periods of time caused the appearance of Sn(II) features in the XPS spectra, thought to be from the formation of Sn_2S_3 due to the removal of sulfur, which indicates that this phase is less stable at elevated temperature. This was also confirmed by visual inspection, which revealed shiny black crystals forming at the edges of the yellow parent ones. This is consistent with the fact that Sn_2S_3 crystals were also found to form in the same ampoule as SnS_2 during growth,[27] and that SnS_2 has been shown to dissociate at higher temperatures, and to form in isolation only at lower temperatures.[21,62]

Core-level XPS

High-resolution spectra of the Sn 3d and S 2p regions were recorded by XPS and fitted using Voigt functions after a Shirley background had been subtracted. A comparison between the Sn $3d_{5/2}$ peaks of the three phases is shown in Figure 1, the corresponding comparison of the S 2p features is shown in Figure 2, and a summary of the fitted binding energies and FWHM of the main core-level features of Sn and S is given in Table 1.

A single, high-intensity Sn $3d_{5/2}$ peak was observed for both the SnS and SnS_2 crystals, with the peak for SnS_2 at 0.9 eV higher binding energy than for SnS. These were assigned to the single oxidation states of tin of Sn(II) and Sn(IV), respectively, and the single, clear, high-intensity peaks in these spectra confirms the phase purity of both materials. Trace amounts of tin oxide remained as a contaminant on both SnS and SnS_2 and is also shown in Figure 1. Although the peak labelled Sn-oxide in the SnS spectrum has similar binding energy to that of Sn^{4+} in SnS_2, the peak is assigned to the oxide because of the observance of its drastic reduction in area after surface cleaning. We note that the oxides forming on SnS and SnS_2 are different in binding energy, however they correspond to the binding energies[63] of SnO on SnS and SnO_2 on SnS_2, which is understandable as there is no change in the oxidation state of tin between these materials and the corresponding oxide.

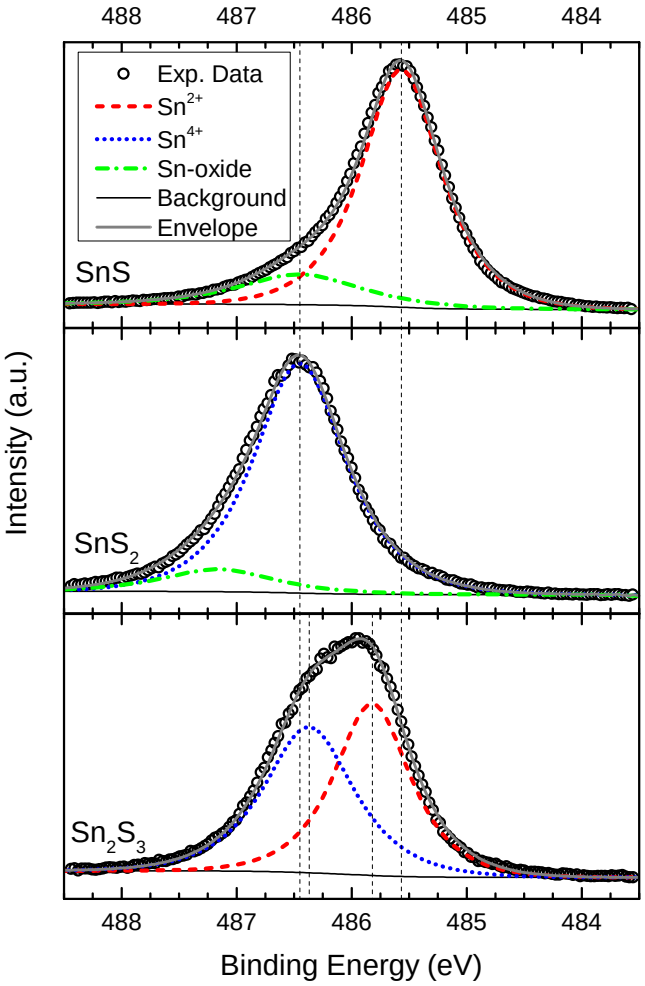

Figure 1. XPS spectra for the Sn $3d_{5/2}$ peak of the clean tin sulfides. Fitted synthetic peaks demonstrate the shift between the different oxidation states of Sn. SnS and SnS_2 showed trace amounts of tin oxide, shown in green.

For Sn_2S_3, the Sn $3d_{5/2}$ spectrum was fitted with two peaks separated by 0.6 eV, which were assigned to the Sn(II) and Sn(IV) oxidation states present in this mixed-valency compound. This assignment is strengthened by the fact that the area ratio was calculated to be 1:1, as expected, and that the FWHM values are comparable to those of the corresponding peaks in the single-valency materials, confirming the expected distribution of tin oxidation states, and providing strong evidence for a phase-pure material. The difference in binding energy of the peaks is, however reduced compared to the single-valency phases; this can be

explained by the fact that the photoemitted electrons from Sn(II) experience a stronger bond due to the presence of Sn(IV) ions, shifting the corresponding Sn $3d_{5/2}$ peak to a higher binding energy, while the converse occurs for electrons photoemitted from Sn(IV) ions, shifting the peak to a lower binding energy.

The S 2p doublet was very well resolved for all three samples, and was fitted using two peaks separated by 1.2 eV with area ratio 1:2, corresponding to the $2p_{1/2}$ and $2p_{3/2}$ features, respectively. It was anticipated that the spectrum for Sn_2S_3 should show two S 2p doublets; however, within the resolution of this study, no further peaks could be resolved and the binding energy shifts are unknown. We therefore report only the binding energy of the S $2p_{3/2}$ peak for each crystal in Table 1, which are in agreement with S in an oxidation state of -2,[37,39] as expected. Trace amounts of sulfur-containing contamination remained on SnS_2 and is also shown in Figure 2. The peaks assigned to these contaminants have binding energies which are in agreement with similar compounds.[64]

The fitted Sn $3d_{5/2}$ binding energies of 485.6 eV and 486.5 eV for SnS and SnS_2, respectively, are in good agreement with other studies of these materials, once the charge referencing methods used are taken into account.[35,37,62,65,66] However, there are also several reports where the results are in stark contrast to those shown here. This is due to a number of issues, including: an unsubstantiated method of charge-referencing based on sulfur;[38,41] a mixed-phase system, believed to be pure;[39,43] a misprint;[21,67] or, most commonly, the reporting of "S 2p" binding energies without resolution into their spin-orbit split components.[38,65,66] There have been few XPS studies of Sn_2S_3, and none have attempted to resolve the two tin oxidation states. These studies do, however, report an enveloping binding energy intermediate of those of the other two phases[38] with a wider FWHM,[40] suggesting that the peak was in fact a convolution of peaks from the two different oxidation states. It is also noted that a lack of attention to the differences in choice of charge reference may have led to the misidentification of oxidation state, and hence phase, in past studies of tin sulfides.[39,40]

Regardless of this, the oxidation states of tin, and therefore the different phases of tin sulfide, can be easily distinguished using properly energy-referenced XPS of a sufficiently high resolution on clean samples. This finding, and a comparison of the XPS spectra of the three phases, have not been reported before, and indicate that XPS can be a useful tool in determining the phase/purity of tin sulfide samples, when appropriately coupled with other phase identification techniques such as XRD and Raman spectroscopy. According to our results, XPS can be reliably used to identify phase-pure SnS or SnS_2, and could be used in conjunction with other techniques to identify Sn_2S_3 or mixed-phase systems. In this way, it can therefore help control single-phase growth of SnS for use in PV applications, and also in the identification of tin sulfide phases forming during the growth of CZTS.

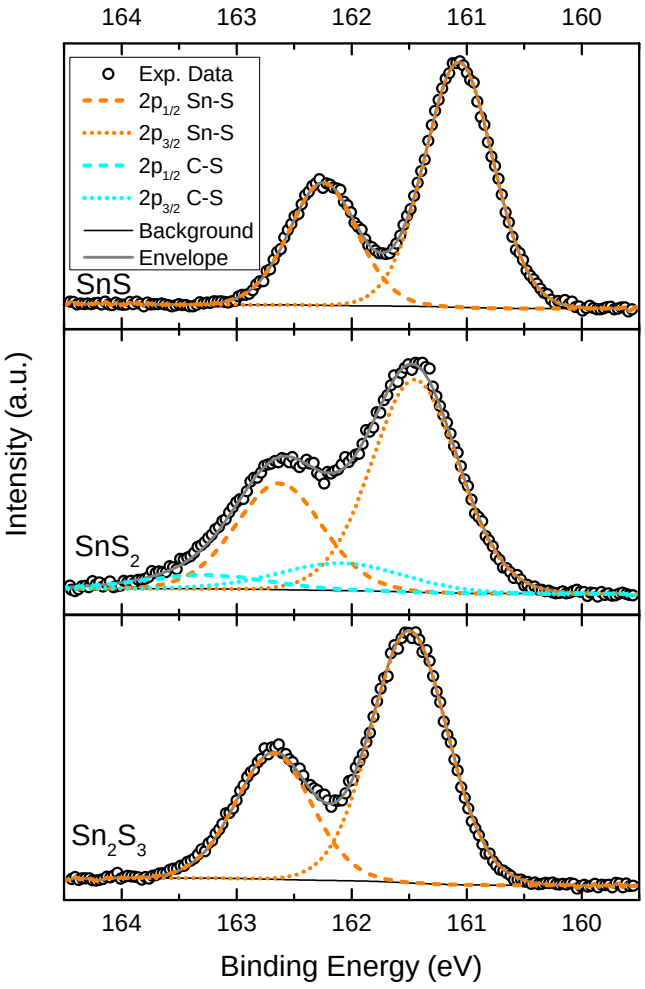

Figure 2. XPS spectra for the S 2p doublet of the clean tin sulfides. SnS_2 showed trace amounts of sulfur-containing contamination, shown in cyan.

Table 1. Fitted Binding Energies of the Main XPS Core-Levels for Clean, Phase-Pure Crystals of SnS, SnS_2 and Sn_2S_3. Peak FWHM values are given in parentheses. All values are given in eV.

Crystal	Sn $3d_{5/2}$		S $2p_{3/2}$
	Sn(II)	Sn(IV)	
SnS	485.6 (0.8)	–	161.1 (0.7)
SnS_2	–	486.5 (0.9)	161.5 (0.9)
Sn_2S_3	485.8 (0.8)	486.4 (0.9)	161.5 (0.8)

Valence Band Spectra

Figure 3 shows the simulated partial density of states (PDoS) curves of the three tin sulfide phases, together with experimentally measured valence band (VB) spectra, obtained from XPS measurements. A Shirley background was subtracted from the latter and includes the Sn 4d core levels, since some VB features are found in the tail of these states. The simulated PDoS curves were corrected using standard photoionization cross-sections,[68] convolved with a Gaussian function (0.41 eV FWHM) to account for ther-

mal broadening and the analyzer response, and then further convolved with a Lorentzian function (0.35 eV FWHM) to account for lifetime broadening. Simulated total DoS curves, obtained by summing the individual PDoS functions, are also shown for direct comparison to the XPS measurements.

The corrected DoS curves are in good agreement with the XPS data for all three phases, with all features present and only slight discrepancies in feature positions and relative intensities. The main discrepancy is found in the high binding energy feature, common to all spectra, which we ascribe to final-state relaxation effects in XPS, which are known to shift features near the bottom of the valence band closer to the valence band edge,[69] and which were not accounted for in the calculations. Also, it has previously been suggested that lifetime broadening increases with binding energy,[69] whereas a constant broadening was used here.

The VB of SnS is comprised of three main features. The first, at 6.5-10 eV binding energy, is dominated by Sn 5s states hybridized slightly with S 3s and 3p states. The second, at 2.5-6.5 eV, is comprised mainly of S 3p states, with a slight contribution from Sn 5p states. The top of the valence band is formed from a hybridization of S 3p and Sn 5s states, with a slight contribution from Sn 5p states. The SnS_2 VB shows two main features, one at 7.5-10 eV, which is dominated by Sn 5s states hybridized slightly with S 3s and 3p states, and a second at 1-7.5 eV, composed of three distinct peaks. Of these, the two at higher binding energy are dominated by S 3p states, with a slight contribution from Sn 5p states, while the largest peak at the top of the valence band is solely due to S 3p states, with no contribution from others. The Sn_2S_3 VB is similarly composed of two main features, the first at 7-10 eV is dominated by Sn 5s states hybridized slightly with S 3s and 3p states, while the second at 1-7.5 eV is similar to the corresponding feature in SnS_2, but with less well-defined peaks. The two peaks at higher binding energy in this region are dominated by S 3p states, with a slight contribution from Sn 5p states, while the most intense peak mainly consists of S 3p states. In contrast to SnS_2, however, there is a shoulder at the top of the valence band, due to a slight hybridization with Sn 5s states.

In the Sn(II) oxidation state, the Sn 5s orbital is occupied and therefore contributes to states at the very top of the valence band; this can be seen in Figure 3 for the spectra of SnS and Sn_2S_3, but is lacking in that of SnS_2. This confirms the expected electronic structure of these materials, i.e. that the top of the valence band for SnS is comprised of a hybridization of cation s and p states, and anion p states, which is in accordance with the lone pair formation mechanism.[70,71] Conversely, for Sn(IV) in SnS_2, the unoccupied Sn 5s orbitals contribute no states to the top of the valence band, and instead contribute empty states to the conduction band, and the valence band in this material is thus dominated by anion p states.

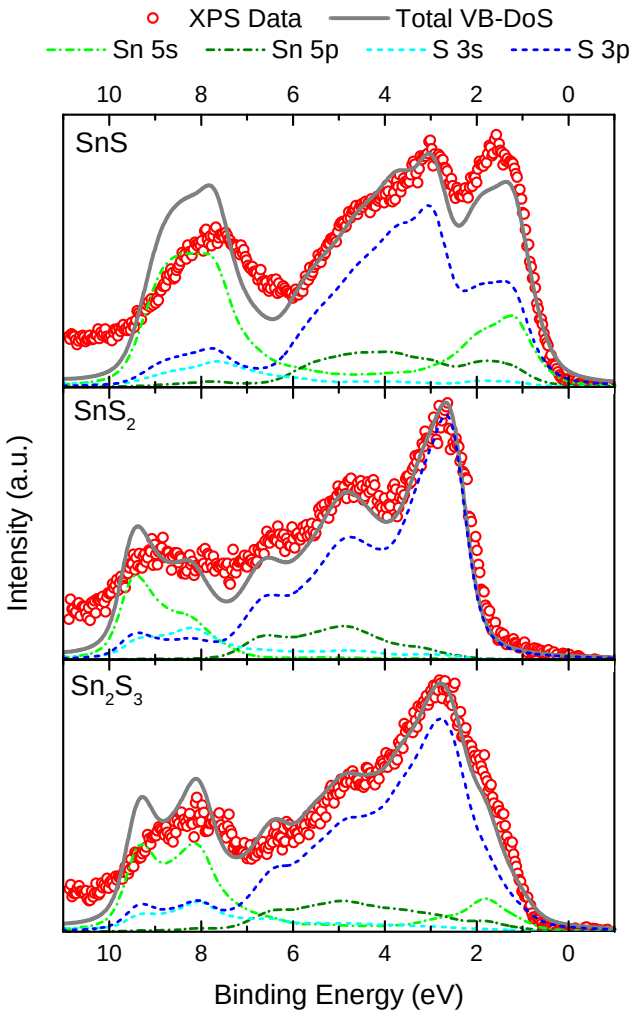

Figure 3. Simulated and measured valence-band spectra for SnS, SnS2 and Sn_2S_3 with respect to the Fermi level at 0 eV binding energy. The experimental data were obtained using XPS, and have been background corrected, while the calculated total and partial DoS curves have been cross-section corrected and broadened for a better comparison to the XPS spectra.

Sn_2S_3 is a true mixed-valency material, with the lone pair hybridization contributing to the top of the valence band, but not as markedly as in SnS, and with the distinctive S 3p feature from SnS_2 also clearly visible.

Simulations of the electronic structures of the three phases have been carried out previously in the literature,[65,72] sometimes with support from XPS measurements,[30,73] and agree well with the results presented here. However, no direct comparison of the DoS and XPS spectra of the three phases has been made,[66] and nor have the contrasting features at the top of the valence band been discussed.[74] We therefore present the first comprehensive comparison of the three phases, employing XPS data and theoretical modeling. By examining the PDoS from the calculations, it can be clearly seen how the hybridization of the Sn lone pair introduces extra states higher in the valence band for SnS, and also how the VB of the mixed-valency Sn_2S_3 is made up of a combination of spectral features

from the single-valency materials, which has not been previously examined directly.[75]

Band Alignment

The combination of XPS and IPES measurements allows the energy-level placements of the valence band maxima (E_{VBM}), conduction band minima (E_{CBM}) and secondary electron cutoff (E_{SEC}) with respect to the Fermi level (E_F) to be obtained. These positions are determined by linear extrapolation of the leading edges of the VB and CB to the baseline. The vacuum level (E_{vac}) can then be placed with respect to E_F by,

$$E_{vac} = E_{SEC} + h\nu,$$

where $h\nu$ is the photon energy.

Hence, the ionization potential (IP) and band gap (E_g) of the materials can be calculated from:

$$IP = E_{vac} - E_{VBM},$$

$$E_g = E_{CBM} - E_{VBM}.$$

The band-edge fitting and corresponding calculated properties for the three phases are shown in Figure 4, with the SEC fittings shown in Figure S13 (Supporting Information). The calculated E_g of 1.06 ± 0.15 eV and IP of 4.71 ± 0.07 eV for SnS are in reasonable agreement with previous studies,[16,27,34,76–80] as is the E_g of 2.28 ± 0.15 eV for SnS_2.[27,32,80–84] The IP of 6.44 ± 0.07 eV for SnS_2 is, however, found to be lower than in other studies[27,76,81,82], possibly due to band-bending effects from slight contamination of the crystal as studied here.[28] For Sn_2S_3, we report a bandgap of 1.10 ± 0.15 eV and an IP of 4.66 ± 0.07 eV. There are comparatively few reports in the literature of the energy levels of this phase, but nevertheless the E_g determined here is in agreement with some previous studies.[27,32] The positions of the Fermi levels in the region probed by the PES measurements are also marked in Figure 4, and the proximity to either the VBM or conduction band minimum (CBM) confirms the expected *p*-type nature of SnS and *n*-type natures of SnS_2 and Sn_2S_3.[85]

By following a vacuum-alignment procedure,[76] we constructed a band-alignment diagram for the three phases (Figure 5), which facilitates both an analysis of the effects of unwanted secondary tin sulfide phase formation within solar cells, and also of the suitability of the three phases of tin sulfide for use in PV applications. Since in this work the crystals were measured in isolation, and the measurement did not take into account any possible band bending, flat bands were drawn and the position of the Fermi level with respect to the bulk band edges is not shown.

It can be seen that SnS and Sn_2S_3 have similar band-level positions, whereas SnS_2 is notably offset to lower energies on the band-alignment diagram. This can be explained by the features seen in the valence-band spectra in Figure 3. The top of the valence band for SnS_2 is dominated by anion p states with no contribution from cation s states. However, for SnS, the Sn 5s orbital is occupied, and due to its hybridization with Sn p and S p orbitals, a filled antibonding orbital occurs at the top of the valence band, higher in energy than the anion p orbital, resulting in a higher offset for SnS. Since Sn_2S_3 is of mixed-valency and displays VB features of both SnS and SnS_2, the same unusual features of the SnS spectrum are also present in this material and therefore Sn_2S_3 exhibits similarly high band positions. This picture accounts for the remarkably low IP of both SnS and Sn_2S_3 compared with SnS_2; although this phenomenon has been noted previously, an explanation in terms of the electronic structure of the materials had not been put forward.

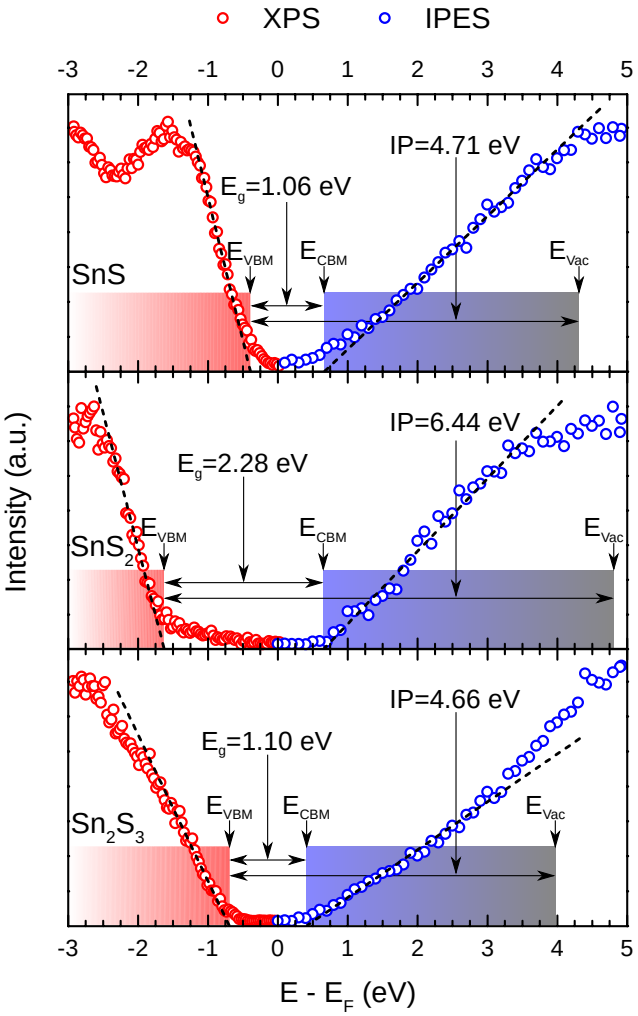

Figure 4. Band edge fitting and energy level determination for the three crystal phases.

The band alignment indicates that the formation of SnS_2 within a SnS solar cell would have a detrimental effect on performance. SnS_2 has a large negative (-0.51 eV) conduction band offset (CBO) with respect to SnS and hence would act as a recombination center.[22] If *n*-type SnS_2 or Sn_2S_3 were to form in CZTS, they could act as a second diode, mitigating the rectifying behavior of the cell. Also, due to its larger bandgap, SnS_2 could also act as an insulator within the cell, inhibiting charge transport.

When compared to other common thin-film PV absorber materials,[86–88] SnS was found to have a relatively low

IP, which, as discussed above, can be explained by the presence of extra states at the top of the valence band. This leads to a band-level mismatch when using common partner materials in a solar cell (such as CdS[89]), confirming previous theoretical work.[25] These results also expand on a previous theoretical study of the band alignment at the CdS/SnS junction,[90] the shortcomings of which include confusion around the correct crystal structure of SnS, and that the band alignment was not referenced to the vacuum level. It is also worth noting that because of its low *IP*, the formation of SnS as a secondary phase in CZTS would affect device performance.

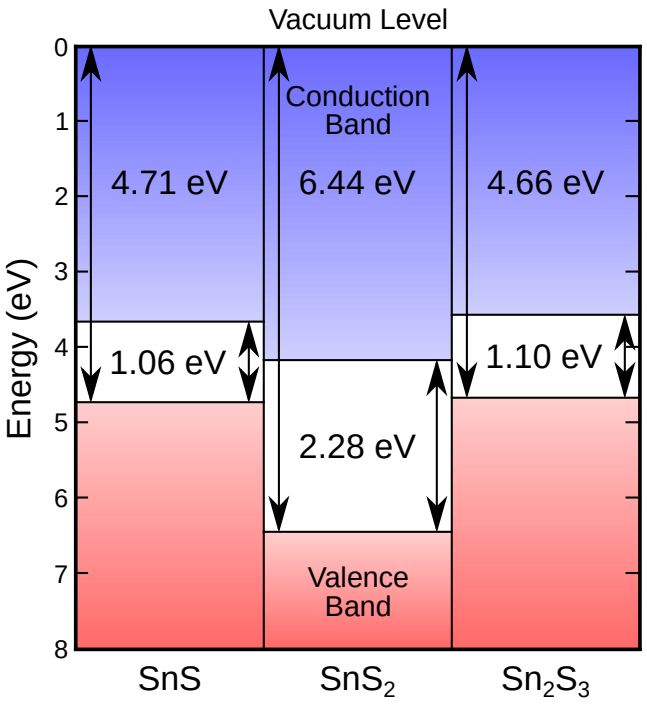

Figure 5. Vacuum-aligned band diagram between the three phases of tin sulfide, with the calculated IP and E_g from XPS/IPES measurements marked.

An attractive proposition is to produce viable PV devices solely from tin sulfide materials. It can be seen from Figure 5 that SnS/SnS_2 and SnS/Sn_2S_3 would form type-*II* heterojunctions; however, a solar cell based on a SnS/SnS_2 junction would be unfeasible due to the aforementioned CBO between them. However, when coupled with a more suitable energy-matched *p*-type absorber, SnS_2 could show promise as a window layer. A cell based on a SnS/Sn_2S_3 junction would seem electronically favorable, with a small positive CBO (0.09 eV), but producing Sn_2S_3 films of consistent quality has been shown to be problematic, depending on growth conditions,[33] and drawing analogy from CIGS, it is likely that a SnS cell would favor a type-*I* heterojunction architecture.[76] The results presented here for the relatively understudied Sn_2S_3 are however, promising for the future development of this material.

CONCLUSIONS

We have demonstrated that a clear identification of the tin sulfide phases SnS, SnS_2, and Sn_2S_3 is possible using XPS, and illustrated the ancillary role that this technique could play in the identification of secondary phases within the PV absorbers SnS and CZTS. Distinct chemical shifts between the two tin oxidation states allow the identification of phase-pure SnS and SnS_2 through XPS alone. XPS/IPES band alignments of the three phases have revealed the potentially detrimental effects on cell performance if secondary phases form within SnS or CZTS films. Proper identification of tin sulfide phases is therefore very important when considering these materials for PV applications, as misidentification could easily lead to confusion during characterization. Furthermore, the agreement between calculated and measured density of states curves for the three phases revealed a distinct difference between the two oxidation states of tin, with additional states present at the top of the valence band for the compounds containing Sn(II), due to the hybridization of the lone pair of electrons in the Sn 5s orbital with the Sn 5p and S 3p orbitals. Such features are not present for the Sn(IV)-containing SnS_2, in which the Sn 5s orbital is unoccupied. These additional states result in a relatively low *IP* for SnS and Sn_2S_3 when compared to SnS_2, and also to other materials commonly used in PV. This offers a new perspective on why SnS cells have thus far achieved only relatively poor performance. Possible uses for SnS_2 and Sn_2S_3 as materials within photovoltaic cells have also been discussed.

ASSOCIATED CONTENT

Supporting Information. Fittings for the secondary electron cutoffs in the XPS data for the three phases of tin sulfide. This material is available free of charge via the Internet at http://pubs.acs.org.

AUTHOR INFORMATION

Corresponding Author

* Email: vin@liverpool.ac.uk

ACKNOWLEDGMENTS

The authors gratefully thank the UK Engineering and Physical Sciences Research Council (EPSRC). T.J.W acknowledges funding through the EPSRC (Grant No. EP/J500471/1) and L.A.B. acknowledges funding from the JSPS (Grant No. 26.04792). J.M.S. and A.W. are supported by the EPSRC (Grant No. EP/K004956/1, EP/L017792/1, and EP/K016288/1). V.R.D. acknowledges support through the Capital for Great Technologies - Grid Scale Energy Storage Programme. T.D.V. acknowledges funding through the EPSRC (Grant No. EP/G004447/2). The computational modelling was carried out primarily using the Balena HPC cluster, maintained by the Bath University Computing Service, with some calculations undertaken on the Archer HPC facility through membership of the UK Materials Chemistry Consortium, which is funded by the EPSRC (Grant No. EP/L000202).

REFERENCES

(1) Delbos, S. Kësterite Thin Films for Photovoltaics : A Review. *EPJ Photovoltaics* **2012**, *3*, 35004.

(2) Wang, W.; Winkler, M. T.; Gunawan, O.; Gokmen, T.; Todorov, T. K.; Zhu, Y.; Mitzi, D. B. Device Characteristics of

CZTSSe Thin-Film Solar Cells with 12.6% Efficiency. *Adv. Energy Mater.* **2014**, *4* (7), n/a – n/a.

(3) Ni, H.-C.; Lin, C.-H.; Lo, K.-Y.; Tsai, C.-H.; Chen, T.-P.; Tsai, J.-L.; Gong, J.-R. Properties of Cu2ZnSnS4 Films by Sulfurization of CuS-SnS-ZnS Precursors Using Ditert-Butylsulfide at Atmospheric Pressure. *ECS J. Solid State Sci. Technol.* **2015**, *4* (8), Q72–Q74.

(4) Fella, C. M.; Romanyuk, Y. E.; Tiwari, A. N. Technological Status of Cu2ZnSn(S,Se)4 Thin Film Solar Cells. *Sol. Energy Mater. Sol. Cells* **2013**, *119*, 276–277.

(5) Thimsen, E.; Riha, S. C.; Baryshev, S. V; Martinson, A. B. F.; Elam, J. W.; Pellin, M. J. Atomic Layer Deposition of the Quaternary Chalcogenide Cu 2 ZnSnS 4. *Chem. Mater.* **2012**, *24* (16), 3188–3196.

(6) Zhang, J.; Long, B.; Cheng, S.; Zhang, W. Effects of Sulfurization Temperature on Properties of CZTS Films by Vacuum Evaporation and Sulfurization Method. *Int. J. Photoenergy* **2013**, *2013*, 1–6.

(7) Scragg, J. J.; Dale, P. J.; Colombara, D.; Peter, L. M. Thermodynamic Aspects of the Synthesis of Thin-Film Materials for Solar Cells. *ChemPhysChem* **2012**, *13* (12), 3035–3046.

(8) Weber, A.; Mainz, R.; Schock, H. W. On the Sn Loss from Thin Films of the Material System Cu–Zn–Sn–S in High Vacuum. *J. Appl. Phys.* **2010**, *107* (1), 013516.

(9) Muska, K.; Kauk, M.; Altosaar, M.; Pilvet, M.; Grossberg, M.; Volobujeva, O. Synthesis of Cu2ZnSnS4 Monograin Powders with Different Compositions. *Energy Procedia* **2011**, *10*, 203–207.

(10) Nagaoka, A.; Yoshino, K.; Taniguchi, H.; Taniyama, T.; Kakimoto, K.; Miyake, H. Growth and Characterization of Cu 2 ZnSnS 4 Single Crystals. *Phys. status solidi* **2013**, *210* (7), 1328–1331.

(11) Koteswara Reddy, N.; Ramakrishna Reddy, K. T. Tin Sulphide Films for Solar Cell Application. In *Conference Record of the Twenty Sixth IEEE Photovoltaic Specialists Conference - 1997*; IEEE, 1997; pp 515–518.

(12) Devika, M.; Reddy, N. K.; Ramesh, K.; Ganesan, R.; Gunasekhar, K. R.; Gopal, E. S. R.; Reddy, K. T. R. Thickness Effect on the Physical Properties of Evaporated SnS Films. *J. Electrochem. Soc.* **2007**, *154* (2), H67.

(13) Tanusevski, A.; Poelman, D. Optical and Photoconductive Properties of SnS Thin Films Prepared by Electron Beam Evaporation. *Sol. Energy Mater. Sol. Cells* **2003**, *80* (3), 297–303.

(14) El-Nahass, M. .; Zeyada, H. .; Aziz, M. .; El-Ghamaz, N. . Optical Properties of Thermally Evaporated SnS Thin Films. *Opt. Mater. (Amst).* **2002**, *20* (3), 159–170.

(15) Koteeswara Reddy, N.; Hahn, Y. B.; Devika, M.; Sumana, H. R.; Gunasekhar, K. R. Temperature-Dependent Structural and Optical Properties of SnS Films. *J. Appl. Phys.* **2007**, *101* (9), 093522.

(16) Vidal, J.; Lany, S.; D'Avezac, M.; Zunger, A.; Zakutayev, A.; Francis, J.; Tate, J. Band-Structure, Optical Properties, and Defect Physics of the Photovoltaic Semiconductor SnS. *Appl. Phys. Lett.* **2012**, *100* (3), 032104.

(17) Sugiyama, M.; Reddy, K. T. R.; Revathi, N.; Shimamoto, Y.; Murata, Y. Band Offset of SnS Solar Cell Structure Measured by X-Ray Photoelectron Spectroscopy. *Thin Solid Films* **2011**, *519* (21), 7429–7431.

(18) Hartman, K.; Johnson, J. L.; Bertoni, M. I.; Recht, D.; Aziz, M. J.; Scarpulla, M. a.; Buonassisi, T. SnS Thin-Films by RF Sputtering at Room Temperature. *Thin Solid Films* **2011**, *519* (21), 7421–7424.

(19) Takeuchi, K.; Ichimura, M.; Arai, E.; Yamazaki, Y. SnS Thin Films Fabricated by Pulsed and Normal Electrochemical Deposition. *Sol. Energy Mater. Sol. Cells* **2003**, *75* (3-4), 427–432.

(20) Ramakrishna Reddy, K. T.; Koteswara Reddy, N.; Miles, R. W. Photovoltaic Properties of SnS Based Solar Cells. *Sol. Energy Mater. Sol. Cells* **2006**, *90* (18-19), 3041–3046.

(21) Schneikart, A.; Schimper, H.-J.; Klein, A.; Jaegermann, W. Efficiency Limitations of Thermally Evaporated Thin-Film SnS Solar Cells. *J. Phys. D. Appl. Phys.* **2013**, *46* (30), 305109.

(22) Sinsermsuksakul, P.; Hartman, K.; Bok Kim, S.; Heo, J.; Sun, L.; Hejin Park, H.; Chakraborty, R.; Buonassisi, T.; Gordon, R. G. Enhancing the Efficiency of SnS Solar Cells via Band-Offset Engineering with a Zinc Oxysulfide Buffer Layer. *Appl. Phys. Lett.* **2013**, *102* (5), 053901.

(23) Steinmann, V.; Jaramillo, R.; Hartman, K.; Chakraborty, R.; Brandt, R. E.; Poindexter, J. R.; Lee, Y. S.; Sun, L.; Polizzotti, A.; Park, H. H.; Gordon, R. G.; Buonassisi, T. 3.88% Efficient Tin Sulfide Solar Cells Using Congruent Thermal Evaporation. *Adv. Mater.* **2014**, *26* (44), 7488–7492.

(24) Sinsermsuksakul, P.; Sun, L.; Lee, S. W.; Park, H. H.; Kim, S. B.; Yang, C.; Gordon, R. G. Overcoming Efficiency Limitations of SnS-Based Solar Cells. *Adv. Energy Mater.* **2014**, *4* (15), n/a – n/a.

(25) Burton, L. A.; Walsh, A. Band Alignment in SnS Thin-Film Solar Cells: Possible Origin of the Low Conversion Efficiency. *Appl. Phys. Lett.* **2013**, *102* (13), 132111.

(26) Burton, L. A.; Walsh, A. Phase Stability of the Earth-Abundant Tin Sulfides SnS, SnS 2 , and Sn 2 S 3. *J. Phys. Chem. C* **2012**, *116* (45), 24262–24267.

(27) Burton, L. A.; Colombara, D.; Abellon, R. D.; Grozema, F. C.; Peter, L. M.; Savenije, T. J.; Dennler, G.; Walsh, A. Synthesis, Characterization, and Electronic Structure of Single-Crystal SnS, Sn 2 S 3 , and SnS 2. *Chem. Mater.* **2013**, *25* (24), 4908–4916.

(28) Burton, L. A.; Whittles, T. J.; Hesp, D.; Linhart, W. M.; Skelton, J. M.; Hou, B.; Webster, R. F.; O'Dowd, G.; Reece, C.; Cherns, D.; Fermin, D. J.; Veal, T. D.; Dhanak, V. R.; Walsh, A. Electronic and Optical Properties of Single Crystal SnS 2 : An Earth-Abundant Disulfide Photocatalyst. *J. Mater. Chem. A* **2016**, *4* (4), 1312–1318.

(29) Sun, Y.; Cheng, H.; Gao, S.; Sun, Z.; Liu, Q.; Liu, Q.; Lei, F.; Yao, T.; He, J.; Wei, S.; Xie, Y. Freestanding Tin Disulfide Single-Layers Realizing Efficient Visible-Light Water Splitting. *Angew. Chemie Int. Ed.* **2012**, *51* (35), 8727–8731.

(30) Bletskan, M. M.; Bletskan, D. I. Electronic Structure of Sn2S3 Compound with the Mixed Valency of Tin. *J. Optoelectron. Adv. Mater.* **2014**, *16* (5-6), 659–664.

(31) Jiang, T.; Ozin, G. A. New Directions in Tin Sulfide Materials Chemistry. *J. Mater. Chem.* **1998**, *8* (5), 1099–1108.

(32) Sanchez-Juarez, A.; Ortiz, A. Effects of Precursor Concentration on the Optical and Electrical Properties of Sn X S Y Thin Films Prepared by Plasma-Enhanced Chemical Vapour Deposition. *Semicond. Sci. Technol.* **2002**, *17* (9), 931–937.

(33) Khadraoui, M.; Benramdane, N.; Mathieu, C.; Bouzidi, A.; Miloua, R.; Kebbab, Z.; Sahraoui, K.; Desfeux, R. Optical and Electrical Properties of Thin Films Grown by Spray Pyrolysis. *Solid State Commun.* **2010**, *150* (5-6), 297–300.

(34) Albers, W.; Haas, C.; Vink, H. J.; Wasscher, J. D. Investigations on SnS. *J. Appl. Phys.* **1961**, *32* (10), 2220.

(35) Cheng, S.; Conibeer, G. Physical Properties of Very Thin SnS Films Deposited by Thermal Evaporation. *Thin Solid Films* **2011**, *520* (2), 837–841.

(36) Ogah, O. E.; Zoppi, G.; Forbes, I.; Miles, R. W. Thin Films of Tin Sulphide for Use in Thin Film Solar Cell Devices. *Thin Solid Films* **2009**, *517* (7), 2485–2488.

(37) Huang, C.-C.; Lin, Y.-J.; Chuang, C.-Y.; Liu, C.-J.; Yang, Y.-W. Conduction-Type Control of SnSx Films Prepared by the Sol–gel Method for Different Sulfur Contents. *J. Alloys Compd.* **2013**, *553*, 208–211.

(38) Cruz, M.; Morales, J.; Espinos, J. P.; Sanz, J. XRD, XPS and Sn NMR Study of Tin Sulfides Obtained by Using Chemical Vapor Transport Methods. *J. Solid State Chem.* **2003**, *175* (2), 359–365.

(39) Balaz, P.; Ohtani, T.; Bastl, Z.; Boldizarova, E. Properties and Reactivity of Mechanochemically Synthesized Tin Sulfides. *J. Solid State Chem.* **1999**, *144* (1), 1–7.

(40) Ettema, A. R. H. F.; Haas, C. An X-Ray Photoemission Spectroscopy Study of Interlayer Charge Transfer in Some Misfit Layer Compounds. *J. Phys. Condens. Matter* **1993**, *5* (23), 3817–3826.

(41) Hernan, L.; Morales, J.; Sanchez, L.; Tirado, J. L.; Espinos, J. P.; Gonzalez Elipe, A. R. Diffraction and XPS Studies of Misfit Layer Chalcogenides Intercalated with Cobaltocene. *Chem. Mater.* **1995**, *7* (8), 1576–1582.

(42) Ichiba, S.; Katada, M.; Negita, H. Mössbauer Effect of 119Sn in the Thermal Decomposition Products of Tin(IV) Sulfide. *Chem. Lett.* **1974**, *2* (9), 979–982.

(43) Morgan, W. E.; Van Wazer, J. R. Binding Energy Shifts in the X-Ray Photoelectron Spectra of a Series of Related Group IVa Compounds. *J. Phys. Chem.* **1973**, *77* (7), 964–969.

(44) Hohenberg, P.; Kohn, W. Inhomogeneous Electron Gas. *Phys. Rev.* **1964**, *136* (3B), B864–B871.

(45) Kohn, W.; Sham, L. J. Self-Consistent Equations Including Exchange and Correlation Effects. *Phys. Rev.* **1965**, *140* (4A), A1133–A1138.

(46) Kresse, G.; Hafner, J. Ab Initio Molecular Dynamics for Liquid Metals. *Phys. Rev. B* **1993**, *47* (1), 558–561.

(47) Perdew, J. P.; Burke, K.; Ernzerhof, M. Generalized Gradient Approximation Made Simple. *Phys. Rev. Lett.* **1996**, *77* (18), 3865–3868.

(48) Grimme, S.; Antony, J.; Ehrlich, S.; Krieg, H. A Consistent and Accurate Ab Initio Parametrization of Density Functional Dispersion Correction (DFT-D) for the 94 Elements H-Pu. *J. Chem. Phys.* **2010**, *132* (15), 154104.

(49) Grimme, S.; Ehrlich, S.; Goerigk, L. Effect of the Damping Function in Dispersion Corrected Density Functional Theory. *J. Comput. Chem.* **2011**, *32* (7), 1456–1465.

(50) Blöchl, P. E. Projector Augmented-Wave Method. *Phys. Rev. B* **1994**, *50* (24), 17953–17979.

(51) Kresse, G.; Joubert, D. From Ultrasoft Pseudopotentials to the Projector Augmented-Wave Method. *Phys. Rev. B* **1999**, *59* (3), 1758–1775.

(52) Monkhorst, H. J.; Pack, J. D. Special Points for Brillouin-Zone Integrations. *Phys. Rev. B* **1976**, *13* (12), 5188–5192.

(53) Krukau, A. V.; Vydrov, O. a.; Izmaylov, A. F.; Scuseria, G. E. Influence of the Exchange Screening Parameter on the Performance of Screened Hybrid Functionals. *J. Chem. Phys.* **2006**, *125* (22), 224106.

(54) Heyd, J.; Scuseria, G. E.; Ernzerhof, M. Hybrid Functionals Based on a Screened Coulomb Potential. *J. Chem. Phys.* **2003**, *118* (18), 8207.

(55) Heyd, J.; Scuseria, G. E.; Ernzerhof, M. Erratum: "Hybrid Functionals Based on a Screened Coulomb Potential" [J. Chem. Phys. 118, 8207 (2003)]. *J. Chem. Phys.* **2006**, *124* (21), 219906.

(56) Blöchl, P. E.; Jepsen, O.; Andersen, O. K. Improved Tetrahedron Method for Brillouin-Zone Integrations. *Phys. Rev. B* **1994**, *49* (23), 16223–16233.

(57) Steichen, M.; Djemour, R.; Gütay, L.; Guillot, J.; Siebentritt, S.; Dale, P. J. Direct Synthesis of Single-Phase P-Type SnS by Electrodeposition from a Dicyanamide Ionic Liquid at High Temperature for Thin Film Solar Cells. *J. Phys. Chem. C* **2013**, *117* (9), 4383–4393.

(58) Sundberg, J.; Lindblad, R.; Gorgoi, M.; Rensmo, H.; Jansson, U.; Lindblad, A. Understanding the Effects of Sputter Damage in W–S Thin Films by HAXPES. *Appl. Surf. Sci.* **2014**, *305*, 203–213.

(59) Velásquez, P.; Ramos-Barrado, J. R.; Leinen, D. The Fractured, Polished and Ar+-Sputtered Surfaces of Natural Enargite: An XPS Study. *Surf. Interface Anal.* **2002**, *34* (1), 280–283.

(60) Loeffler, M. J.; Dukes, C. A.; Chang, W. Y.; McFadden, L. A.; Baragiola, R. A. Laboratory Simulations of Sulfur Depletion at Eros. *Icarus* **2008**, *195* (2), 622–629.

(61) Nossa, A.; Cavaleiro, A. Chemical and Physical Characterization of C(N)-Doped W–S Sputtered Films. *J. Mater. Res.* **2004**, *19* (08), 2356–2365.

(62) Reddy, M. V.; Babu, P.; Ramakrishna Reddy, K. T.; Miles, R. W. X-Ray Photoelectron Spectroscopy and X-Ray Diffraction Studies on Tin Sulfide Films Grown by Sulfurization Process. *J. Renew. Sustain. Energy* **2013**, *5* (3), 031613.

(63) Köver, L.; Moretti, G.; Kovács, Z.; Sanjinés, R.; Cserny, I.; Margaritondo, G.; Pálinkás, J.; Adachi, H. High Resolution Photoemission and Auger Parameter Studies of Electronic Structure of Tin Oxides. *J. Vac. Sci. Technol. A Vacuum, Surfaces, Film.* **1995**, *13* (3), 1382.

(64) Lindberg, B. J.; Hamrin, K.; Johansson, G.;Gelius, U.; Fahlman, A.; Nordling, C.; Siegbahn, K. Molecular Spectroscopy by Means of ESCA II. Sulfur Compounds. Correlation of Electron Binding Energy with Structure. *Phys. Scr.* **1970**, *1* (5-6), 286-298.

(65) Ettema, A. R. H. F.; de Groot, R. A.; Haas, C.; Turner, T. S. Electronic Structure of SnS Deduced from Photoelectron Spectra and Band-Structure Calculations. *Phys. Rev. B* **1992**, *46* (12), 7363–7373.

(66) Martinez, H.; Auriel, C.; Loudet, M.; Pfister-Guillouzo, G. Electronic Structure (XPS and Ab-Initio Band Structure Calculation) and Scanning Probe Microscopy Images of α-Tin Sulfide. *Appl. Surf. Sci.* **1996**, *103* (2), 149–158.

(67) Ahmet, I. Y.; Hill, M. S.; Johnson, A. L.; Peter, L. M. Polymorph-Selective Deposition of High Purity SnS Thin Films from a Single Source Precursor. *Chem. Mater.* **2015**, *27* (22), 7680–7688.

(68) Yeh, J. J.; Lindau, I. Atomic Subshell Photoionization Cross Sections and Asymmetry Parameters: $1 \leqslant Z \leqslant 103$. *At. Data Nucl. Data Tables* **1985**, *32* (1), 1–155.

(69) Ley, L.; Pollak, R. a.; McFeely, F. R.; Kowalczyk, S. P.; Shirley, D. a. Total Valence-Band Densities of States of III-V and II-VI Compounds from X-Ray Photoemission Spectroscopy. *Phys. Rev. B* **1974**, *9* (2), 600–621.

(70) Walsh, A.; Payne, D. J.; Egdell, R. G.; Watson, G. W. Stereochemistry of Post-Transition Metal Oxides: Revision of the Classical Lone Pair Model. *Chem. Soc. Rev.* **2011**, *40* (9), 4455.

(71) Walsh, A.; Watson, G. W. Influence of the Anion on Lone Pair Formation in Sn(II) Monochalcogenides: A DFT Study. *J. Phys. Chem. B* **2005**, *109* (40), 18868-18875.

(72) Parker, D.; Singh, D. J. First Principles Investigations of the Thermoelectric Behavior of Tin Sulfide. *J. Appl. Phys.* **2010**, *108* (8), 083712.

(73) Lefebvre, I.; Lannoo, M.; Olivier-Fourcade, J.; Jumas, J. C. Tin Oxidation Number and the Electronic Structure of SnS-In2S3-SnS2 Systems. *Phys. Rev. B* **1991**, *44* (3), 1004–1012.

(74) Lorenz, T.; Joswig, J.-O.; Seifert, G. Combined SnS@SnS 2 Double Layers: Charge Transfer and Electronic Structure. *Semicond. Sci. Technol.* **2014**, *29* (6), 064006.

(75) Lefebvre, I.; Lannoo, M.; Moubtassim, M. E.; Fourcade, J. O.; Jumas, J.-C. Lithium Insertion in Three-Dimensional Tin Sulfides. *Chem. Mater.* **1997**, *9* (12), 2805–2814.

(76) Sugiyama, M.; Shimizu, T.; Kawade, D.; Ramya, K.; Ramakrishna Reddy, K. T. Experimental Determination of Vacuum-Level Band Alignments of SnS-Based Solar Cells by Photoelectron Yield Spectroscopy. *J. Appl. Phys.* **2014**, *115* (8), 083508.

(77) Banai, R. E.; Burton, L. A.; Choi, S. G.; Hofherr, F.; Sorgenfrei, T.; Walsh, A.; To, B.; Cröll, A.; Brownson, J. R. S. Ellipsometric Characterization and Density-Functional Theory Analysis of Anisotropic Optical Properties of Single-Crystal α-SnS. *J. Appl. Phys.* **2014**, *116* (1), 013511.

(78) Sun, L.; Haight, R.; Sinsermsuksakul, P.; Bok Kim, S.; Park, H. H.; Gordon, R. G. Band Alignment of SnS/Zn(O,S) Heterojunctions in SnS Thin Film Solar Cells. *Appl. Phys. Lett.* **2013**, *103* (18), 181904.

(79) Zainal, Z.; Hussein, M. Z.; Ghazali, A. Cathodic Electrodeposition of SnS Thin Films from Aqueous Solution. *Sol. Energy Mater. Sol. Cells* **1996**, *40* (4), 347–357.

(80) Engelken, R. D. Low Temperature Chemical Precipitation and Vapor Deposition of SnxS Thin Films. *J. Electrochem. Soc.* **1987**, *134* (11), 2696.

(81) Zhuang, H. L.; Hennig, R. G. Theoretical Perspective of Photocatalytic Properties of Single-Layer SnS2. *Phys. Rev. B* **2013**, *88* (11), 115314.

(82) Schlaf, R.; Pettenkofer, C.; Jaegermann, W. Band Lineup of a SnS2/SnSe2/SnS2 Semiconductor Quantum Well Structure Prepared by van Der Waals Epitaxy. *J. Appl. Phys.* **1999**, *85* (9), 6550.

(83) Amalraj, L.; Sanjeeviraja, C.; Jayachandran, M. Spray Pyrolysised Tin Disulphide Thin Film and Characterisation. *J. Cryst. Growth* **2002**, *234* (4), 683–689.

(84) Shi, C.; Chen, Z.; Shi, G.; Sun, R.; Zhan, X.; Shen, X. Influence of Annealing on Characteristics of Tin Disulfide Thin Films by Vacuum Thermal Evaporation. *Thin Solid Films* **2012**, *520* (15), 4898–4901.

(85) Sánchez-Juárez, A.; Tiburcio-Silver, A.; Ortiz, A. Fabrication of SnS2/SnS Heterojunction Thin Film Diodes by Plasma-Enhanced Chemical Vapor Deposition. *Thin Solid Films* **2005**, *480-481*, 452–456.

(86) Walsh, A.; Chen, S.; Wei, S.-H.; Gong, X.-G. Kesterite Thin-Film Solar Cells: Advances in Materials Modelling of Cu2ZnSnS4. *Adv. Energy Mater.* **2012**, *2* (4), 400–409.

(87) Teeter, G. X-Ray and Ultraviolet Photoelectron Spectroscopy Measurements of Cu-Doped CdTe(111)-B: Observation of Temperature-Reversible CuxTe Precipitation and Effect on Ionization Potential. *J. Appl. Phys.* **2007**, *102* (3), 034504.

(88) Hinuma, Y.; Oba, F.; Kumagai, Y.; Tanaka, I. Ionization Potentials of (112) and ($11\bar{2}$) Facet Surfaces of CuInSe2 and CuGaSe2. *Phys. Rev. B* **2012**, *86* (24), 245433.

(89) Li, Y.-H.; Walsh, A.; Chen, S.; Yin, W.-J.; Yang, J.-H.; Li, J.; Da Silva, J. L. F.; Gong, X. G.; Wei, S.-H. Revised Ab Initio Natural Band Offsets of All Group IV, II-VI, and III-V Semiconductors. *Appl. Phys. Lett.* **2009**, *94* (21), 212109.

(90) Ichimura, M. Calculation of Band Offsets at the CdS/SnS Heterojunction. *Sol. Energy Mater. Sol. Cells* **2009**, *93* (3), 375–378.

ToC Artwork

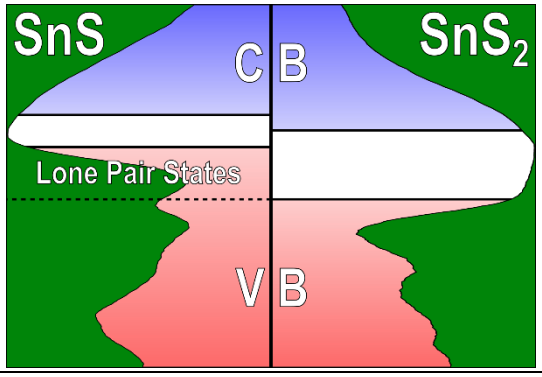

SUPPORTING INFORMATION

Band Alignments, Valence Bands and Core Levels in the Tin Sulfides SnS, SnS_2 and Sn_2S_3: Experiment and Theory

Thomas J. Whittles[†], Lee A. Burton[‡], Jonathan M. Skelton[§], Aron Walsh[§], Tim D. Veal[†], Vin R. Dhanak*[,†]

[†]Stephenson Institute for Renewable Energy, University of Liverpool, Liverpool L69 7ZF, UK

[‡]Structure and Materials Laboratory, Tokyo Institute of Technology, 4259 R3-7 Nagatsuta, Midori-ku, Yokohama 226-8503, Japan

[§]Centre for Sustainable Chemical Technologies, Department of Chemistry, University of Bath, Bath BA2 7AY, UK

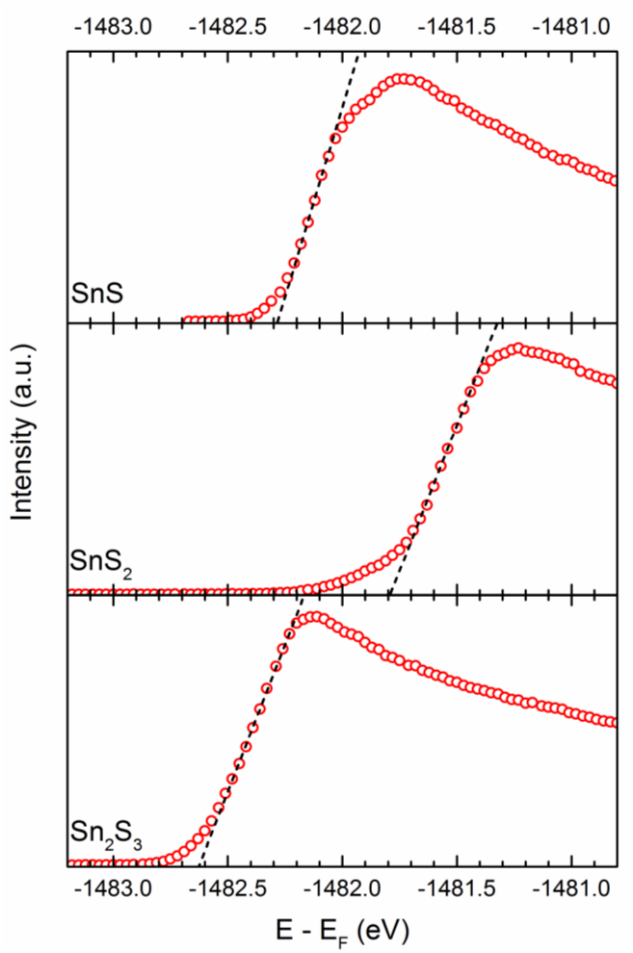

Figure S1. Secondary electron cutoffs for the XPS spectra of SnS, SnS_2 and Sn_2S_3, showing the linear extrapolation fits to the baselines.